

A NEW METRIC TO ANALYZE PROPAGATION MODELS

J. Blas, R. M. Lorenzo, P. Fernández, and E. J. Abril

Department of Signal Theory, Communications and Telematics
Engineering
University of Valladolid, Campus Miguel Delibes
Camino del Cementerio s/n, Valladolid 47011, Spain

A. Bahillo, S. Mazuelas, and D. Bullido

Center for the Development of Telecommunications of Castilla y León
CEDETEL, Edificio Solar, Parque Tecnológico de Boecillo
Boecillo (Valladolid) 47151, Spain

Abstract—Deterministic propagation models are typically validated by performing comparisons between real and simulated E -field envelope distributions. These distributions correspond to straight spatial segments and, occasionally, also surfaces. This approach is correct to study large scale fading for relatively large distances. However, in a real environment and shorter distances, there are too many details to consider. As a result, it is almost impossible to reach a point by point match in a minimally realistic experiment. There are two ways to deal with this problem. The first one is to model every minor detail everywhere around us, keeping the point by point metric. The second one is to change that metric in order to admit, at least in part, that we can not take into account of all the details. If uncertainty can not be eliminated, we should learn to take advantage of it by using a statistical metric like the one proposed here. This paper uses such a kind of metric to validate several structural and geometrical simplifications of a model for the transition between outdoor and indoor propagation that has been recently published. Furthermore, we demonstrate that this metric has helped us to improve and understand better this model, while revealing unexpected model properties at the same time.

Corresponding author: J. Blas (juabla@tel.uva.es).

1. INTRODUCTION

Every propagation problem requires a detailed description of reality. However, even relatively exhaustive numerical models that allow you to include a fine-grained media description, such as finite difference time domain (FDTD), introduce some kind of averaging. In fact, there is no alternative to assign proper material properties to finite-difference modeling grids when the model has features that are smaller than the grid size [1]. In general, the vast majority of real problems needs some kind of averaging. However, this averaging does not always mean a loss of accuracy [2]. In addition, not all the elements that are present in the simulation volume have to be described with the same level of detail. Although it is necessary to minimize the loss of accuracy, it is also important to simplify the description of reality. This simplification is possible when we identify the key elements of the problem and focus our efforts on getting the optimum level of detail.

In order to identify the key model elements and to compare their relative importance, we need a simple case. In particular, as we want to model the transition between outdoor and indoor propagation, we choose an empty room with only one exterior wall. Of course, it is not really empty, since there is an operator to perform measurements. However, as the human body is an important obstacle at 900 MHz, he was placed far from the facade, close to the opposite wall, while he kept an eye in the automatic measurement process. The room model is an idealization, we do not take into account of neither geometric details such as pillars, wall irregularities, doors, etc. nor inhomogeneities such as the several materials in ceiling, wall and floor. We employ perfect electric conductor boundary conditions; the numerical room acquires a cuboid shape and we also eliminate wall thickness.

As a result, it is impossible to obtain a point by point fit among the measurements and the simulations performed in a region under test which consists of several thousands of sampling points. The usual metric is completely useless, because the standing wave pattern amplitude on each point depends on the exact path length, attenuation and phase of an undetermined number of contributions. We should also note that the emitting source is a log-periodic dipole array (LPDA) which has not a proper phase center and produces low cross-polarization levels. Even more, as the transmitter antenna is behind a window and inside another room (in turn a resonant cavity), the effective antenna is not the LPDA but the window aperture where the signal is passing through. As a result, we should take into account not only details inside the room, but also some important external ones, such as the metal covers on the window frame joints in the

building which is in front of our empty room, because those metal covers scatter the energy that the empty room facade reflects back toward the transmitter facade.

Therefore, in order to develop and validate the model, it is absolutely crucial to select a metric capable of identifying the influence of each contribution on the final measured interference pattern. This metric should allow us to tune independently each of the contributions and to choose the optimal accuracy level for the environment description. A point by point metric simply cannot do that. Of course, the human capacity to identify this kind of relationships just by visual inspection is extremely limited. The capacity of analyzing a model by studying the parameter space with such a metric is highly valuable. This metric can be employed with many propagation models; it is not specific of our model. This last point is what really gives relevance to the present work, since although the model is also interesting by itself it is not a general model but just a relatively specific one.

Image reconstruction by means of inverse scattering problem is a highly nonlinear and ill-posed problem [3,4]. But a direct electromagnetic field intensity map of scattering sources has proved to be useful for target recognition [5–7]. While analyzing the model parameter space, we will also study the description of the emitting source that arises from the seek for its center of phase. In particular, this description is inferred from the results obtained while altering the hypothetical position for the model source point. The agreement with the real setup is highlighted even more when exact spherical wave attenuations are employed instead of a local plane wave approximation.

2. PROPAGATION MODEL CONTEXTUALIZATION

Our aim is to determine how sensitive our model is to variations in its parameter values and its structure. The understanding of how the model behaves in response to changes in its input, is of fundamental importance to ensure a correct use. Model parameters are twofold. Some of them describe the geometry of the problem:

- Room dimensions: height, depth and width.
- Window panes size and position: height, width; distance to lateral walls, floor and ceiling.
- Transmitter position and wavelength: three coordinates are used to specify the position.

While the others are specific of this type of propagation model:

- Sub-aperture number: we keep the aperture aspect ratio.

- Sub-aperture distance with respect to the window panes (window sill effect).
- Maximum recursion depth in the method of images: there are 3 recursion depth indexes. First, lateral walls, floor and ceiling provide a matrix of images and therefore two indexes. Second, the remaining walls are considered by means of parallel repetitions of the previous matrix.

In order to achieve accurate results both of them are important. However, robustness against small errors in parameter specification enhances the usefulness of the model given that in many cases it is not easy nor practical to obtain a precise measure of these quantities.

Before going any further, let us briefly recall the experimental setup that we presented in [8] when we first discussed this model, since we will employ it again to study the model parameter space. Some important additional information such as floor and elevation plans can be found there. The room where we carried out the measurement is represented in Fig. 1. The two windows on the back of the room are illuminated by an exterior 900 MHz signal without modulation, which comes from another room which is almost in front of the previous one. These two rooms are in different wings of an E-shape building but

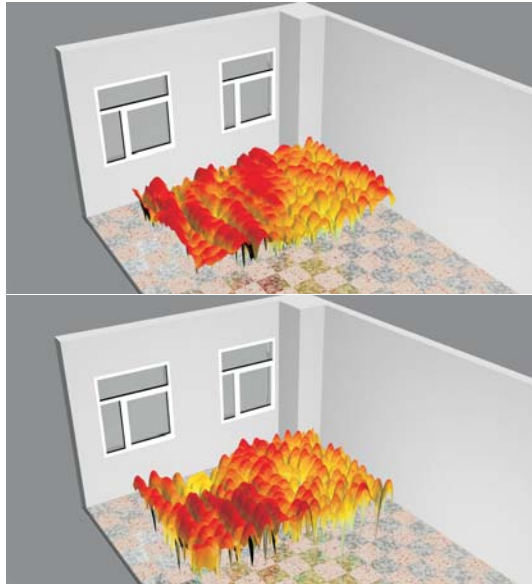


Figure 1. *E*-field envelope [dB], vertical polarization. Comparison between experimental and simulated distributions (in that order).

on the same floor. A log-periodic dipole array (LPDA) emits vertical polarization through the window of the transmitting room. The results correspond to the envelope of the E -field vertical component. On the top we show the experimental results and below it the simulated ones. The spatial sampling rate was 0.06λ in the first case and 0.1λ in the second one.

Standing waves are clearly visible in Fig. 1. Some effects of them on small animals enclosed in metallic boxes have been recently reported in [9]. The main peaks of the field envelope appear near the bottom left corner of the region under test (RUT). They arise as a consequence of the interaction of two principal contributions: the direct beam coming from the right window and a reflected beam, originated in the left window but coming from the left lateral wall. Nevertheless, this wall is suppressed for clarity in Fig. 1. The interference produces two clear peak alignments, parallel to the lateral walls, while the rest of the peaks seem not to follow a regular pattern. However, there also exists a region under the right window where the peaks are closely spaced. Besides, the spatial variations are less pronounced than in other places. This region reveals a dominant contribution due to one of the windows.

We should also address some clear deviations of the simulations and the measurements in proximity to the windows, especially the local minimum of the electrical field close to the right corner of the left window. Such a difference is a logical consequence of the model simplifications. In particular, two approximations are especially relevant in this case. The first one is that there exists a pillar on the left corner in the real room, similar to the pillar visible in Fig. 1. Both pillars are completely ignored in the simulations. However, the left pillar is being directly illuminated by the exterior source, so scattering processes change the local spatial energy distribution near this corner in the real room. The second important difference is the presence of another building wing, just in front of the windows: after two bounces the energy penetrates into the room almost perpendicularly by travelling along the shortest path between the facades, reaching the referred position of the local minimum in the simulation.

In spite of these and other differences, the Kolmogorov-Smirnov test (KS-test) between the real and simulated cumulative distribution functions (CDF) provides a p -value around 0.99. This p -value is the probability that one would actually observe such a maximum difference between both CDFs, given that both sets of samples come from the same distribution. If we could find an appropriate random generator, p -values should occur evenly between 0.0 and 1.0. In contrast, our model assigns consistently high p -values when the source points are located on a position which corresponds to the real source position.

The conclusion is clear; there is a deterministic relationship between both number generators: the real propagation phenomena and our model. However, in order to reveal these properties, a big enough area needs to be considered, otherwise geometrical details such as pillars or other unexpected contributions can hide this underlying relationship. Of course, although KS-test can be applied to any number of samples it is much more descriptive when there are a large number of them.

Standing wave patterns are a superposition of energy fluxes with different directions. The standing wave ratio (SWR) is an indicator of the balance between these energy fluxes. Therefore, our model can have in average an statistical interference pattern quite similar to the real one, although some of the energy fluxes are deviated. It could be interpreted as a consequence of the energy conservation law. Anyway, reaching a 99% is not the same as reaching a 100%; there is some margin to improve the characterization. Our model is not perfect, but its level of accuracy is very adjusted to the level of detail included. Much more detailed models based on ray-tracing or ray-tracing/FDTD yield worse results as demonstrated in [8].

Anyway, our model could increase the level of detail, including materials, furniture, and so on, exactly in the same way that ray-tracing does. Ray-tracing has proved to be useful for outdoor and indoor modeling. In contrast, we are studying the transition between outdoor and indoor propagations so we do not focus on this kind of problems. We simplify the problem to understand better what is generally happening. Please also note that the model does not use absolute values because we are studying relative variations in the spatial E -field distribution. So other minor contributions such as propagation through the facade wall are not taken into account. In short, it is the empty space characterization which makes the room model useful.

3. STATISTICAL DISTRIBUTION VARIATIONS

A variety of statistical models of envelope distributions, such as Rayleigh, Rician, Nakagami-m, Weibull, etc., have been proposed. These distributions are different expressions of the same underlying phenomenon under diverse physical conditions. In fact, there exist some unifying approaches such as the spherically-invariant random processes (SIRP) and the α - μ distribution [10, 11]. They are general fading distributions including many of the other distributions as particular cases. In [8], we pointed out that our model was able to fit a Rayleigh distribution. However, this is one of the most basic models: it appears when the phases of the individual interfering waves are

random, but the time delays are approximately equal for all of them. The question naturally arises whether the new model would cope with more general distributions apart from the Rayleigh one. To answer this question the discussion will be centered on the experiment that we reported in [8]. In that paper, we showed that the simulation was able to fit the experimental cumulative distribution function (CDF) with accuracy under controlled experimental conditions and now we go deeper into the specific statistical distribution that appears.

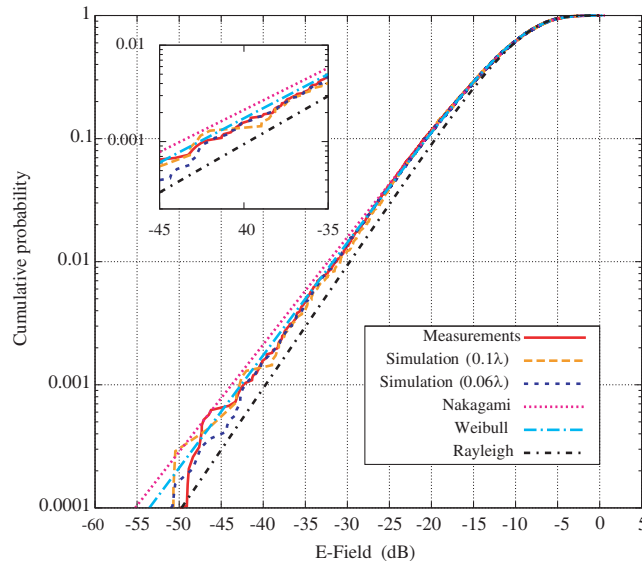


Figure 2. Comparison with well-known fading distributions by using the maximum likelihood estimator. Simulation data corresponding to two different spatial sampling rates are provided.

In Fig. 2, we show the relationship among experimental data, simulated data and some important fading distributions. Nakagami-m and Weibull distributions fit the experimental data quite well. Nakagami fading occurs when multipath scattering with relatively large time-delay spreads gives rise to different clusters of reflected waves. The envelope of each cluster signal is Rayleigh distributed. Rayleigh-fading signals appear as the resultant of a large number of signals having the same delay and arbitrary phase. Hence, we can consider the Rayleigh fading as a particular case of Nakagami fading. Consequently, our model seems to be able to simulate cluster aggregation and not only the behavior of isolated clusters. Apart from that, our model fits the empirical distribution better than the Weibull or Nakagami-m

distributions. More complex distributions mentioned at the beginning of this section, such as the α - μ distribution or SIRP, have not been tested. Since their physical meaning is not clearly stated, they do not add useful information to interpret our results.

The maximum likelihood estimation provides a Nakagami- m distribution whose p -value is 0.82. We must note that this p -value is overestimated due to the fact that the Nakagami- m parameters have been directly derived from the experimental data. Anyway it demonstrates that this Nakagami- m is an excellent random generator in order to build the real distribution. In contrast, the p -value in our model is consistently around 0.99, because it is a deterministic generator, not a random one. It can follow with great detail the overall cluster distribution of this particular problem.

Another issue is the sampling rate influence of the simulation on the CDF. In Fig. 2, we show two simulated CDFs. In particular, we increase the sampling rate from 0.1λ to 0.06λ , matching the sampling rate of the experimental setup. It can be appreciated that increasing the overall number of simulated samples provides a better fit for lower values. The inset of Fig. 2 shows a detailed view of this region. The simulation follows the real distribution closely till CDF values approach 0.1%.

4. SUB-APERTURE NUMBER AND SOURCE INTENSITY MAPS

One of the structural parameters of our model is the number of sub-apertures employed to represent each window pane of the externally illuminated room. As the window pane is divided into a rectangular grid of sub-apertures, it is necessary to specify the number of sub-apertures per row (H) and per column (V). In this section, we will set out that choosing non optimal (H, V) values does not lead to completely different results but it introduces some kind of distortion.

In Fig. 3, we can see the p -value obtained if we place our hypothetical point source in different points of the window surface from which the transmitter antenna was emitting. Each point on the p -value surface corresponds to the model output when the center of phase of the emitting source is precisely fixed in that point. As H and V reach the highest values (see the last three plots in Fig. 3) the contour lines approach a limit distribution. However, this limit distribution does not provide the best fit. There are mainly two problems: the high p -value region is shifted to the right and p -values are lower in general than in the third case ($H = V = 3$). Anyway we must also note that all the cases have a wide area with p -values over 10% and bear some

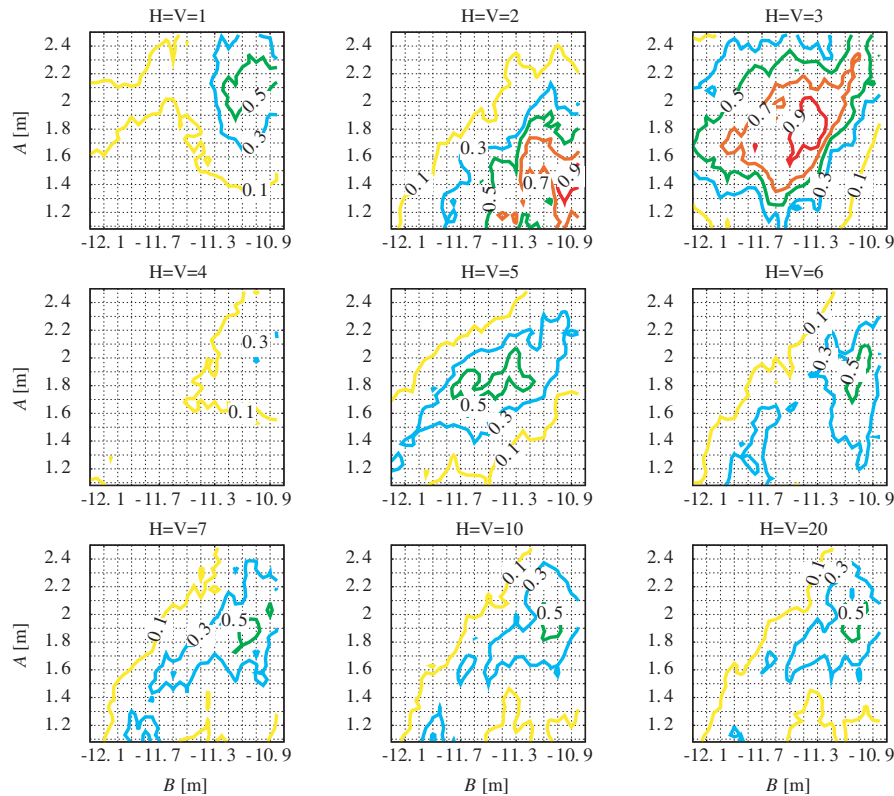


Figure 3. Comparison among different (H, V) values. Each graph shows the p -values obtained assuming that the center of phase of the transmitter is located in several points of the window where the source signal was passing through.

resemblance. In particular, they place just a local maximum inside the window surface and the p -value tends to decay progressively from this peak to the rest of the area. It is also interesting to note that the plots get better as they approach $(H = V = 3)$ except for the case $(H = V = 4)$. Let us recall that $(H = V = 3)$ keeps the sub-apertures as big as possible without violating far field condition in the region under test.

Another important discussion would be the hypothetical reason of the lack of symmetry around the peak p -value. In fact, the contour lines on the left of the peak area are more spaced out than they are on the right. This is specially clear for $(H = V = 3)$. This interesting and unexpected p -value distribution can be explained taking into account

of the orientation of the transmitting antenna and making a more in-depth analysis of the nature of the effective radiation source. Modeling of nearest antenna vicinity is crucial to understand the real antenna directional pattern [12–14]. In our case, the source incorporates basically two elements: the antenna and the window from which the antenna was emitting. It is also important to note that the emitter and the receiver are inside different rooms.

The primary source is a log-periodic dipole array (LPDA) with vertical polarization. Its axis is parallel to the ground but it is not perpendicular to the transmitting window, having an angle of incidence around 30° on the window pane. For antennas such as horn, LPDA, and others, an ideal phase center position available in entire space does not exist [15, 16]. We can imagine that we are in a street in the dark and suddenly someone turns a torchlight on behind a window in a building room. Although the torchlight beam is illuminating us, we also see some additional clarity around the main beam, through the window panes. In the Fig. 3, specially for $(H = V = 3)$, the p -value map shows an analogous picture of the LPDA. The other (H, V) cases suffer from distortion.

The results presented in Fig. 4 are the consequence of a small structural model change. We have added spherical wave attenuation to the model source point; therefore the illumination amplitude now is not uniform for each sub-aperture as before. We take into account of small path length variations among them and the source point. The result is a sharper picture of the LPDA for all the (H, V) cases. The important idea is that we do not rely just on one p -value to measure the model accuracy but we employ a whole picture of the real source to perform a comparison. The better is the picture, the better is the model. Reversely, this metric can classify how much weight each contribution has in the final interference pattern, which is not less important to debug the model.

In the last figures, the source position has been limited to the transmitting window surface. In Fig. 5, we add volume clipping to show the 3D volumetric data set. In particular, we have added two surfaces: the horizontal clipping plane is parallel to the floor, and the vertical clipping plane shows the azimuthal angle of incidence. Their intersection contains the axis of the transmitting antenna. As it is shown, the simulation provides a clear detection of the transmitting antenna axis.

5. INFLUENCE OF ROOM GEOMETRICAL DESCRIPTION

Figure 6 illustrates p -value variations due to changes in the perpendicular direction to the window wall. In particular, the horizontal axis shows different hypothetical distances between the plain of the apertures and the opposite wall, that is to say room depth plus window sill depth. In addition, vertical axis shows hypothetical distances between the apertures and the region under test. Note that although we change the simulation entry data, the real measurements are unperturbed, and therefore not all the hypothesis produce the same

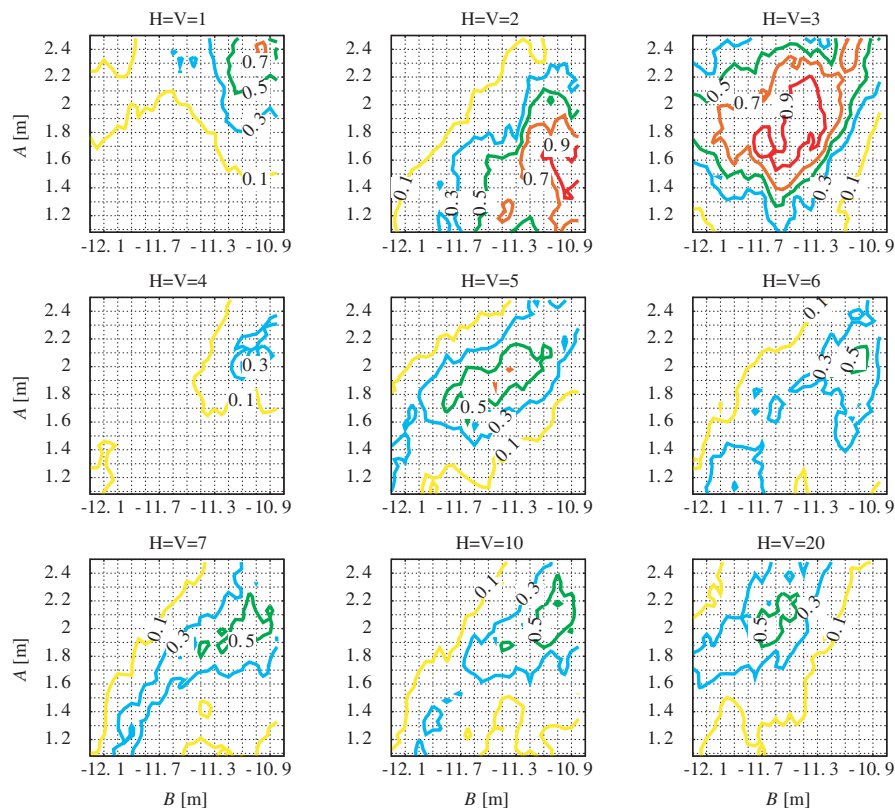


Figure 4. Comparison between different H, V values. Each graph shows the p -values obtained assuming that the center of phase of the transmitter is situated in different points of the window where the source signal was passing through.

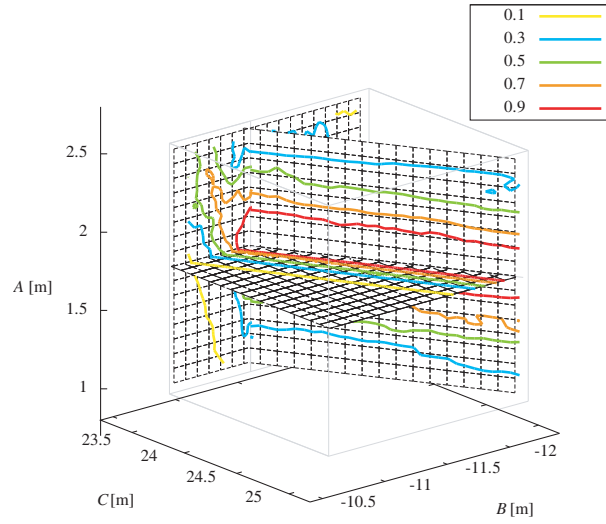


Figure 5. Influence of source position on p -value. Volume clipping for $H = V = 3$. The AB surface is on the transmitting window. The intersection of the other two surfaces is the line where the transmitting antenna axis was placed.

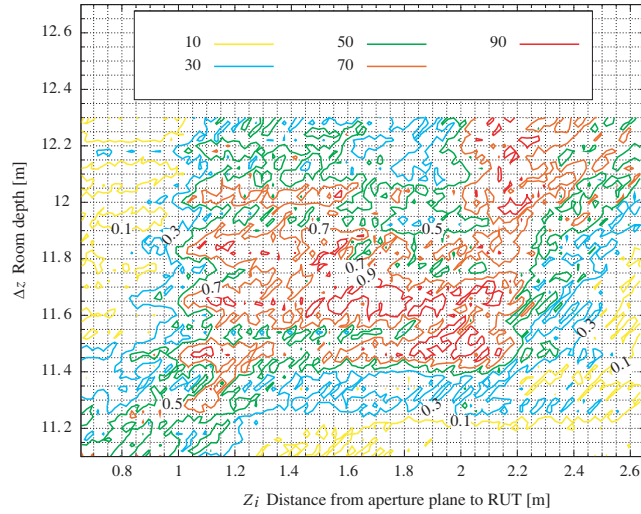


Figure 6. P -value variations due to changes in the values of room depth and region under test (RUT) proximity to the window apertures.

results. There are two purposes for Fig. 6: first, to find out how precise should be the value of these lengths to achieve accurate results, and second, to demonstrate that the aperture plain should be placed in the outer plane of the window wall.

Let us begin with the discussion about whether to include window sill depth in room depth or not, and therefore whether the apertures are to be considered to lay on the outer or inner surfaces of the window wall. We should recall that the real window sill depth is around 30 cm. So if we consider that the aperture plain is on the inner window wall surface, we must subtract this length from the room depth. Accordingly, the new depth should be around 11.35 m. However, in Fig. 6 this hypothetical room depth does not provide results as accurate as the ones obtained including the window sill depth in the room depth. Nevertheless, the real room depth is not a constant, as can be seen in the floor plan. So to remove this doubt we should also use the vertical axis of the Fig. 6 to corroborate our affirmation. In this axis, we show the result of moving the region away from apertures keeping the region height from the room floor constant. If we do not include the window sill the real value would be around 1.4 m, which again has worse results than those obtained considering the apertures on the outer surface of the window wall.

The discussion regarding to precision intends to show the influence of erroneous room dimensions on the results. In Fig. 6, we can distinguish a central area with higher p -values, close to 99%. Its width is 10 cm, which represents a 1% error in the room depth value. In addition, we have also changed the recursion level for the electric images to include some reflection in the inner surface of the wall which contains the real windows. Till now, there have been just two parallel planes of images in the model, the first including the real apertures and the second adding the opposite wall effects; now we have added a third one. As expected, there have been not great variations, the p -value has decreased from 0.99 to 0.92. Consequently, the minor effect of this reflection can not be modeled by using the PEC model for the entire wall, because the windows distort this behavior. Although we employ perfect electric conductor boundary conditions, we also use a finite number of images. This is an implicit way to take into account of power absorption and transmission by walls. This parameter could be adjusted in order to take into account of different kinds of materials.

Among the different geometrical parameters that represent the room, those that describe window apertures are especially important, since they control the location and radiation pattern of the sources and its electric images. Fig. 7 shows the effect of shifting each of the two windows as a whole on the same plane where they lay. In the left

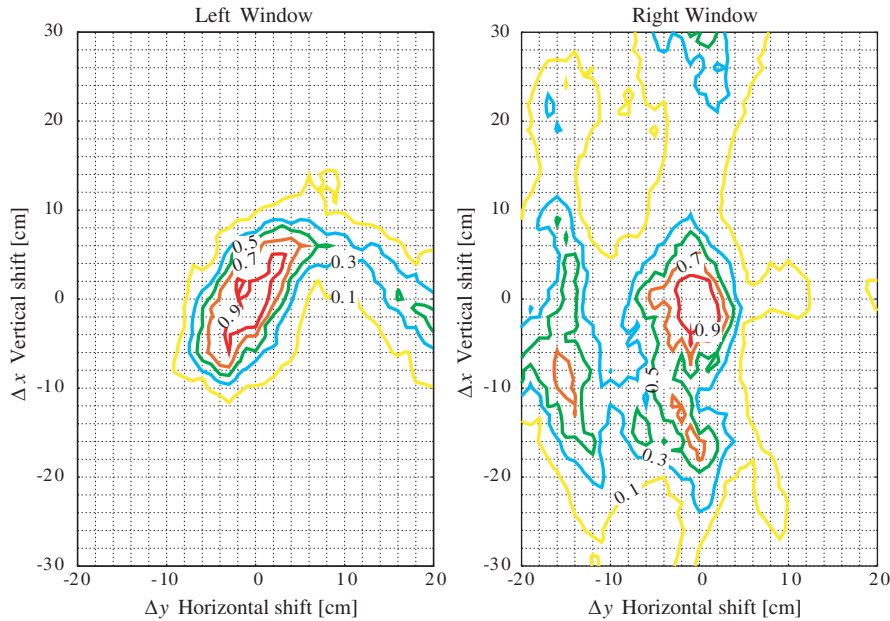


Figure 7. Influence of windows shift on p -value.

graph, the right window is kept fixed and we move the left window, while in the right graph it is the left window which stays still and the right one is moved. Positive values in the vertical axis mean an upward movement, while the negative ones mean a downward movement. If we were inside the room looking at the windows, the negative values in the horizontal axis would indicate, for example, a window displacement to our left.

The areas which present the highest p -values are centered on the middle of the graphs of Fig. 7. Therefore, our efforts to measure these parameters with especial accuracy seem to have yielded good results, given that the theoretical model is consistent with the measures for a relatively narrow range of values. In that sense, the left window demonstrates to be more restrictive than the right one. This contrast could be explained by taking into account of the presence of a pillar close to the left window. The pillar is directly illuminated by the exterior source through this window, although we do not take it into account. Its presence does not significantly modify the overall E -field statistics but it limits the parameter range of valid values for the window position.

In addition to window position analysis, we present a complementary discussion about window size influence. The first thing to note is

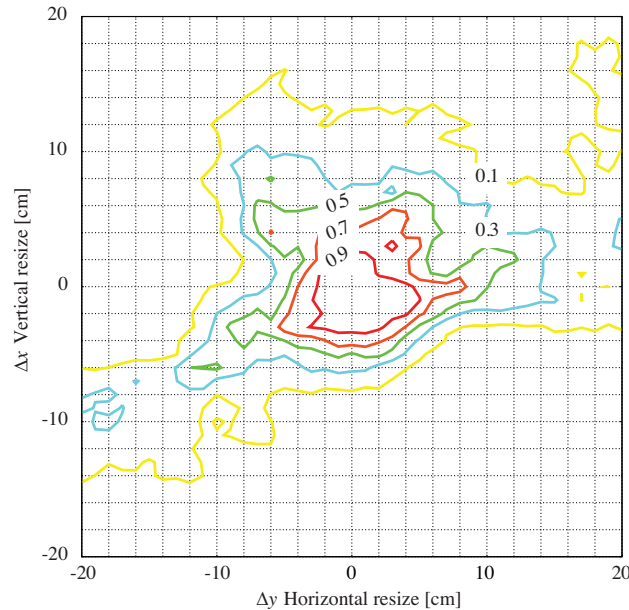


Figure 8. Dependence of p -value on windows size. The increments are applied twice. If the window were a circle the increment would be the radius increment. They are applied to both windows at the same time.

that each window is composed of three panes of glass mounted in aluminum frames. If the window numerical model is simplified by using just one pane per window, ignoring the internal frames, the model loses its accuracy. Furthermore, subsequent changes in the sub-aperture number do not improve the results. So, we will change the size of the windows keeping their internal frames and the window center unmodified, stretching just the outer lines which bound each window.

The dependence of p -value on window size can be appreciated in Fig. 8. There is a reasonable area in parameter space that provides good p -values. Therefore, in this case we can also confirm that the good behavior is not a spike but an gradual improvement obtained when model parameters approach their real values and consequently, small deviations from real values are admissible.

Finally, Fig. 9 presents the influence of deviations in the height and width of the room model respect to the real ones. One of the important model parameters is precisely the distance of the measurement points to the walls, ceiling and floor. As it can be appreciated, there is a relatively narrow range of possible values. In comparison with window

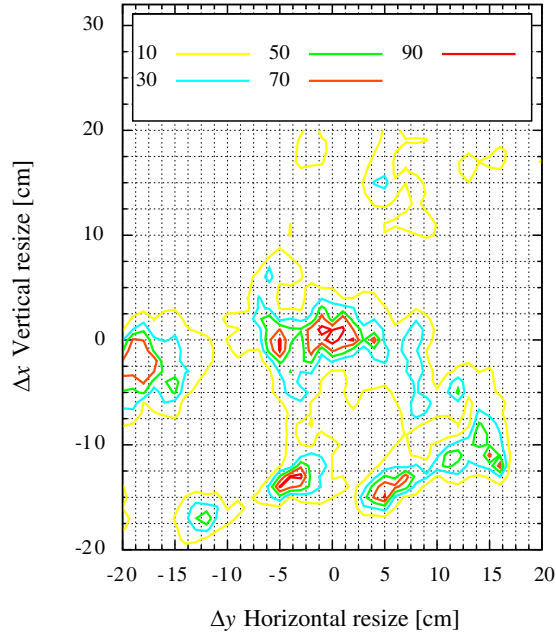


Figure 9. Influence of room cross-section size on p -value. The increments are applied twice. If the cross-section were a circle, the increment would be a radius increment.

size measures, these other measures are more important. Besides, we should not forget that the pillars are not considered and this also makes the valid parameter range narrower.

Now, we are in conditions of reviewing again the E -field envelope comparison of Fig. 1. We are going to compare visually the measures, the correct sub-aperture model simulation and a bad approximation. The bad approximation is the result of performing a simulation eliminating the frame influence. As it can be observed in Fig. 10, the two simulated interference patterns look quite similar. However, the bad approximation provides a much lower p -value ($5.52E - 7$ instead of 0.99). As a final conclusion, this metric can detect many important errors unnoticed by the human eye. Even more, this powerful tool can be employed with any other propagation method, such as ray-tracing for example.

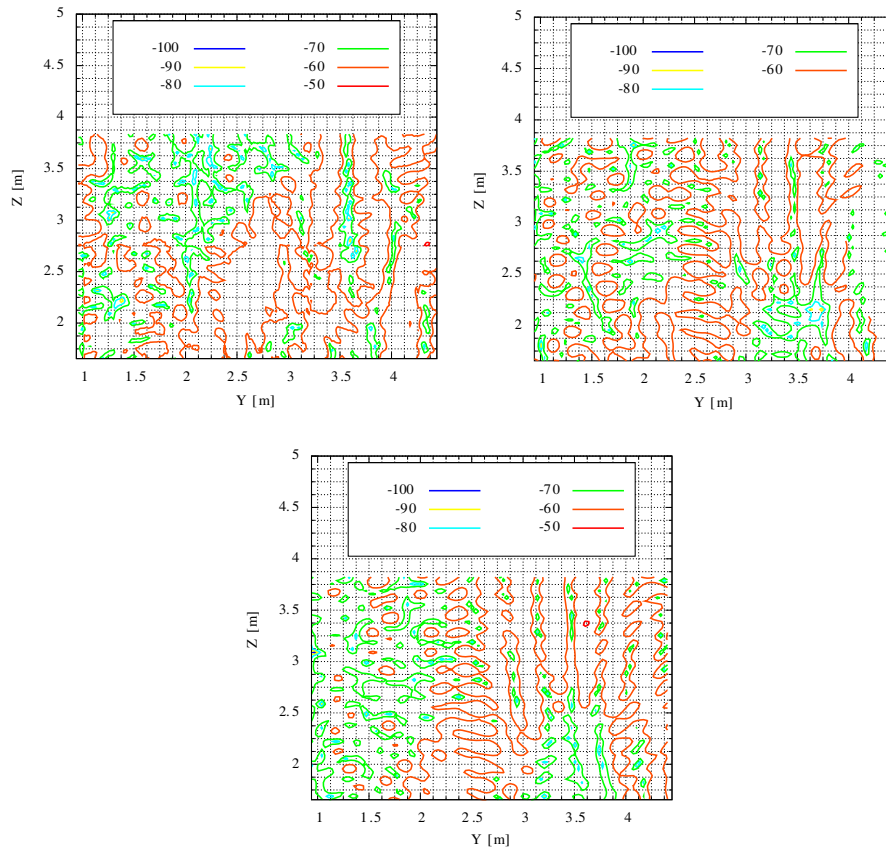


Figure 10. Comparison among the E -field distributions on the RUT obtained by measurements and simulations. There are two simulations: only one is correct, the other has a severe structural error (p -value = $5.52E - 7$).

6. CONCLUSIONS

After analyzing the sub-aperture propagation model, the following conclusions can be drawn out. The sub-aperture model involves a geometrical description of the environment, but not all the surrounding objects are equally important, nor their description needs the same level of detail to get accurate results. The windows are the more important parameters because they act like primary sources in the receiver room. The geometrical description of the window panes must be accurate. For example, it is necessary to take into account that

each window is divided into three panes; the internal frames can not be suppressed. After all, this conclusion is logical because the window is the basic building block of the model. Each window is replicated many times due to image theory, so a bad window characterization induces bad results. The model seems to be less sensitive to the geometrical description of the room, since apparently important details such as pillars or lack of regularity on the opposite wall are compatible with a good fit between the measured and simulated CDFs.

The simplification of the problem geometry and material description makes it impossible to predict the field pattern on a point by point basis. It is remarkable that, in spite of the local deviations, the overall statistics provide an accurate fit. This fit is not a fortuitous result in the parameter space and corresponds to an accurate description of the main elements of the real environment. At the same time, the predicted pattern presents a close resemblance with the real pattern in general terms. In particular, the model reproduces aligned patterns close to the wall which is being illuminated, while there are other areas where a chaotic alignment is achieved. Those chaotic alignments are not easy to obtain. They were obtained only when the model was correctly implemented. There also exist other areas under the effect of just one window with a reduced spatial variability that appear in the simulation. Therefore, the model can imitate several local spatial profiles in order to follow the global real behavior. The comparison among the simulated CDFs and well-known standard distributions unveils that the model can describe accurately not only problems with a dominant cluster but also problems that include diverse clusters. Moreover, it can characterize the real CDF although there are no basic distributions that fit the real data so closely as the model. Increasing the spatial sampling rate of the simulated field yields a better fit for the lower field values.

The model employs a point source as emitter, while the real emitter is a log-periodic dipole array just behind the window of another exterior room distinct from the room where the field distribution has been measured. Consequently, the effective emitter is the aperture created by this window. If the point source is placed in different points of this aperture, the results exhibit higher p -values associated to the areas with more intense illumination inside this aperture. The asymmetry in the intensity distribution due to the angle of the log-periodic antenna respect to the emitting window is reproduced in the p -value profile. In short, the model seems to provide an intensity map of this emitting aperture. In addition, the direction of arrival to the receiver room can be identified by extending the point source p -value analysis to the volume behind the emitting aperture. The model can

establish the relationship between secondary radiation sources and the real measurements.

In order to validate some structural decisions in the model, the alternative hypothesis have been tested. In particular, the sub-apertures that represent the windows of the room under test could have been placed in the plane which lies in the inner wall surface. However, the p -value clearly increases when the sub-apertures are situated on the outer surface of the window wall. The selection of the optimal number of sub-apertures is important but it does not produce a complete degradation in the results. However, it distorts them by decreasing the maximum p -value achieved and shifting its position. Increasing the number of sub-apertures gives a convergent solution but the better results are obtained by keeping as few sub-apertures as possible while respecting the far-field condition. The geometrical simplifications of the room are also discussed and they do not significantly perturb the results, but they have effects on the valid parameter space.

Another structural modification applied to the model was to include a particularized path loss attenuation for each sub-aperture based on their exact path length. Till now, we had employed a constant path loss for all the sub-apertures. As the path length differences involved are quite small, this modification resulted in a small perceptible refinement of calculated fields by increasing the areas where a hypothetical point source can contribute to the final solution. The most important aspect is that such a small detail, that we know for sure that it is correct, can improve the results in a so perceptible way. This fact demonstrates a fine adjustment between the model and the intrinsic properties of wave propagation.

We must point out that we have used a new metric to perform the systematic tuning of the model. This metric provides an in-depth analysis of individual contributions and allows us to select a balanced level of detail. Each description is as simple as it can be in order to obtain accurate results. Even more, we have found which the key elements are. These principles are of general applicability and they can be employed to adjust any other propagation model.

ACKNOWLEDGMENT

The authors want to thank the reviewers for their comments and suggestions, which helped us to improve the final manuscript. This work was supported in part by the Regional Ministry for Public Works of the Junta de Castilla y León.

REFERENCES

1. Habashy, T. M. and A. Abubakar, "A generalized material averaging formulation for modelling of the electromagnetic fields," *Journal of Electromagnetic Waves and Applications*. Vol. 21, No. 9, 1145–1159, 2007.
2. Tan, C.-P., J.-Y. Koay, K.-S. Lim, H.-T. Ewe, and H.-T. Chuah, "Classification of multi-temporal SAR images for rice crops using combined entropy decomposition and support vector machine technique," *Progress In Electromagnetics Research*, PIER 71, 19–39, 2007.
3. Zhong, X.-M., C. Liao, W. Chen, Z.-B. Yang, Y. Liao, and F.-B. Meng, "Image reconstruction of arbitrary cross section conducting cylinder using UWB pulse," *Journal of Electromagnetic Waves and Applications*, Vol. 21, No. 1, 25–34, 2007.
4. Huang, C.-H., Y.-F. Chen, and C.-C. Chiu, "Permittivity distribution reconstruction of dielectric objects by a cascaded method," *Journal of Electromagnetic Waves and Applications*. Vol. 21, No. 2, 145–159, 2007.
5. Park, S. H., K. K. Park, J. H. Jung, H. T. Kim, and K. T. Kim, "Construction of training database based on high frequency RCS prediction methods for ATR," *Journal of Electromagnetic Waves and Applications*, Vol. 22, 693–703, 2008.
6. Ma, C.-Z., T. S. Yeo, H. S. Tan, and G. Lu, "Interferometric ISAR imaging on squint model," *Progress In Electromagnetics Research Letters*, Vol. 2, 125–133, 2008.
7. Park, S. H., K. K. Park, J. H. Jung, H. T. Kim, and K. T. Kim, "ISAR imaging of multiple targets using edge detection and Hough transform," *Journal of Electromagnetic Waves and Applications*, Vol. 22, 365–373, 2008.
8. Blas, J., P. Fernández, R. M. Lorenzo, E. J. Abril, S. Mazuelas, A. Bahillo, and D. Bullido, "A model for transition between outdoor and indoor propagation," *Progress In Electromagnetics Research*, PIER 85, 147–167, 2008.
9. López-Martín, E., J. C. Bregains, F. J. Jorge-Barreiro, J. L. Sebastián-Franco, E. Moreno-Piquero, and F. J. Ares-Pena, "An experimental set-up for measurement of the power absorbed from 900 MHz GSM standing waves by small animals, illustrated by application to picrotoxin-treated rats," *Progress In Electromagnetics Research*, PIER 87, 149–165, 2008.
10. Yao, K., M. K. Simon, and E. Biglieri, "A unified theory

- on wireless communication fading statistics based on SIRP,” *Fifth IEEE Workshop on Signal Processing Advances in Wireless Communications*, 2004.
11. Yacoub, M. D., “The α - μ distribution: A physical fading model for the stacy distribution,” *IEEE Transactions on Vehicular Technology*, Vol. 56, 27–34, 2007.
 12. Sukharevsky, O. I. and A. Y. Shramkov, “High-frequency method of antenna directional pattern calculation,” *Journal of Electromagnetic Waves and Applications*, Vol. 21, No. 14, 2009–2023, 2007.
 13. Sukharevsky, O. I. and V. A. Vasilets, “Scattering of reflector antenna with conic dielectric radome,” *Progress In Electromagnetics Research B*, Vol. 4, 159–169, 2008.
 14. Oğuzer, T. and A. Altintas, “Free content analysis of the nonconcentric reflector antenna-in-radome system by the iterative reflector antenna and radome interaction,” *Journal of Electromagnetic Waves and Applications*, Vol. 21, No. 1, 57–70, 2007.
 15. Wang, Y., J. Wang, Z. Zhao, and J. Yang, “A novel method to calculate the phase center of antennas,” *Journal of Electromagnetic Waves and Applications*, Vol. 22, No. 2/3, 239–250, 2008.
 16. Green, H. E., “The phase centre of a pure mode, smooth wall, conical horn,” *Progress In Electromagnetics Research B*, Vol. 4, 285–298, 2008.